Supplementary Information

Elucidating a Key Anti-HIV-1 and Cancer-Associated Axis: The Structure of CCL5 (Rantes) in Complex with CCR5

Phanourios Tamamis and Christodoulos A. Floudas*

Department of Chemical and Biological Engineering, Princeton University, NJ, USA

***Corresponding Author:** Christodoulos A. Floudas

Department of Chemical and Biological Engineering, Princeton University, Princeton, NJ, 08544

Phone: 609-258-4595; Fax: 609-258-0211; email: floudas@titan.princeton.edu

Supplementary Discussion

Schnur *et al.*[1] have recently biosynthesized a soluble CCR5 ectodomain composed of unsulfated N-terminal CCR5 domain, extracellular loop 1 and 2 and synthesized chimeric peptides containing disulfated-N-terminal CCR5 domain conjugates with extracellular loops 1 and 3, as well as, a conjugate of extracellular loops 1 and 2. These peptides, together with N-terminal CCR5 domain as a control, were used to map the interactions of between the N-terminal and extracellular domains of CCR5 with CCL5. Also in a previous study, Schnur *et al.*[2] used NMR studies to derive a conformation for the 7-23 residue fragment of the CCR5 N-terminal domain.

In our study, we used the conformation derived in the previous study of Schnur *et al.*[2] to model the complete CCR5 structure, the validity of which is demonstrated by the exceptional agreement with experimental findings, in the investigation of the entire CCR5, in complex with (i) a dual tropic HIV-1 gp120 V3 loop[3], and (ii) CCL5 (present study). In addition, the computationally derived structure of this study, which utilized NMR conformations of CCL5[4,5] , depicts that the N-terminal domain of CCL5 forms crucial interactions with the CCR5 transmembrane domain, in line with experiments[6,7,8,9,10,11]. Within the simulation, the C-terminal 56-68 residue domain of CCL5 is not proximal to the CCR5 N-terminal domain and extracellular loops of CCR5; the distance of CCL5 Met67 Cα – CCR5 Pro19 Cα, which is the closest CCR5 residue from CCL5 residue Met67, is within 19-21 Å. Combining (i) the knowledge gained from previous experimental findings investigating the entire chemokine and chemokine receptor complex (showing that the N-terminal domain of CCL5 penetrates into the transmembrane region of CCR5), as well as the computationally derived structure derived here, and (ii) the experimental evidence for the high structural integrity of both the CCR5 transmembrane domain[12] and the region of CCL5 outside the N-terminal domain[5], our study suggests that it is structurally-geometrically infeasible for CCL5 residues Met67 and Ser68 to interact with CCR5 (when CCL5 binds to the entire CCR5). CCL5 residues Met67 and Ser68 were affected by the binding to CCR5 constructs composed only by the (i) N-terminal domain – extracellular loop 1 – extracellular loop 2, and (ii) extracellular loop 1 – extracellular loop 2[1].

The similarity between (i) the important CCL5 residues in residue moiety 12-50 which according to our study they mainly interact with the N-terminal domain of CCR5, and (ii) the CCL5

residues which according to Schnur *et al.*[1] are affected owing to the CCL5 binding to the N-terminal domain of CCR5 only, suggests that CCL5 in[1] could presumably have acquired a more proper binding and relative orientation with regard to the N-terminal domain, in the presence of the N-terminal domain only, compared to the experimental assays where extracellular loops were present. As the present study, as well as previous experiments[6,7,8,9,10,11], provide evidence on the crucial role of the CCR5 transmembrane domain in binding and signaling, it is possible that its absence[1] – specifically in the experimental assays which included extracellular loops 1 and 2 – has affected negatively the correct binding and relative orientation of CCL5 with regard to the chimeric peptides.

Supplementary Methods

Analysis of Complex 14A: We analyzed the intermolecular interaction free energies between CCL5 and CCR5 residue pairs of the simulation snapshots in Complex 14A using Supplementary Equation (1):

$$\Delta G_{RR'}^{\text{inte}} = \underbrace{\sum_{i \in R} \sum_{j \in R'} \left(E_{ij}^{\text{Coul}} + E_{ij}^{\text{GB}} \right)}_{\Delta G_{RR'}^{\text{polar}}} + \underbrace{\sum_{i \in R} \sum_{j \in R'} E_{ij}^{\text{vdW}} + \sigma \sum_{i \in R, R'} \Delta S_i}_{\Delta G_{RR'}^{\text{non polar}}} \qquad \text{(Supplementary Equation 1)}$$

The first and second group of terms on the right-hand side of Supplementary Equation 1 describe, respectively, polar and non-polar interactions between R and R'. A similar methodology for the analysis of interacting residues has been used for the elucidation of the molecular recognition of CXCR4 CCR5 by a dual tropic V3 loop[3,13], the molecular recognition of CXCR4 by CXCL12[14], the delineation of problems related to species specificity of proteins[15], the design of transgenic proteins[16], and in problems related to drug design[17,18,19]. In the calculations, R corresponds to a CCL5 residue and R' to a CCR5 residue. To compute the GB term in Supplementary Equation (1), we included all atoms and set the charges of atoms outside the two – under investigation – residues R and R' to zero. The last term contains the difference in solvent accessible surface areas of residues R and R' in the complex and unbound states. The generalized-Born energies and the atomic accessible-surface areas (ΔS_i) entering in Supplementary Equation 1 depend on the location of R and R' in the complex. The polar component contains a Coulombic term and a GB contribution, modeling the interaction between residue R and the solvent polarization potential induced by R' (or vice versa). Similarly, the non-polar component contains a van der Waals interaction between R, R' and a surface term, expressing cavity contributions and nonpolar interactions with the surrounding solvent. The non-polar and polar solvation terms were calculated using the heterogeneous water-membrane-water GBSW[20] using the same parameters as in[3,13]. The sum of the two components, polar and non-polar, reflects the total direct interaction between R and R' in the solvated complex. Subsequently, we decomposed the polar and non-polar interaction free energy contributions and present the results of the average intermolecular interaction free energies of the lowest binding free energy complex in two dimensional density maps in Supplementary Figure 1. In addition, we summed up the total intermolecular interaction free energies of every CCR5 residue, so as to provide insights into the role of each interacting CCR5 residue with CCL5 (first column per CCR5 residue in Figure 3), and the results are

presented in Figure 3. Also, in Figure 3, we provide a comparison to the sum of intermolecular interaction free energies summed up for every CCR5 residue with regard to the HIV-1 gp120 V3 loop binding (second column per CCR5 residue in Figure 3) using data from Tamamis and Floudas[3].

CCR5 Interacting Residues in Complex with CCL5 versus HIV-1 gp120 V3 loop:

We summed up the residue pair-wise interaction free energies for every CCR5 residue in complex with (i) CCL5 (first column of Figure 3 per CCR5 residue) and (ii) the dual tropic HIV-1 gp120 V3 loop of[3] (second column of Figure 3 per CCR5 residue). Figure 3 presents the total interaction free energies of CCR5 residues which possess at least -4.5 kcal/mol total interaction free energy in at least one of the two complexes (i) or (ii), and is partitioned in panels (A) and (B). If a CCR5 residue interacts strongly and approximately equally with both CCL5 and the HIV-1 gp120 V3 loop, it is listed in panel A, whereas, if a CCR5 interacts strongly with CCL5 and weakly with the HIV-1 gp120 V3 loop, or vice versa, it is listed in panel B. To quantify if a j-th (j ∈ 1,352) CCR5 residue interacts strongly with both CCL5 and the HIV-1 gp120 V3 loop (e.g. it belongs to panel A), we used the expression in Supplementary Equation (2) as a criterion:

$$\frac{\left| \sum_{q=1}^{N(residues\ of\ CCL5)} \Delta G_{q,j}^{inte} - \sum_{p=1}^{M(residues\ of\ HIV-1\ gp120\ V3\ Loop)} \Delta G_{p,j}^{inte} \right|}{\left| \min\left(\sum_{q=1}^{N(residues\ of\ CCL5)} \Delta G_{q,j}^{inte}, \sum_{p=1}^{M(residues\ of\ HIV-1\ gp120\ V3\ Loop)} \Delta G_{p,j}^{inte} \right) \right|} < 0.75 \qquad \text{(Supplementary Equation 2),}$$

where $\Delta G_{i,j}^{inte}$ in Supplementary Equation (2) denotes the interaction free energy between residue j of CCR5 and any interacting residue i of either CCL5 (i=q in Eq(1)) or the HIV-1 gp120 V3 loop (i=p in Supplementary Equation (2)). For any values greater or equal than 0.75, the CCR5 residue is listed in panel B. Based on the results, the choice of 0.75 proved to be appropriate for categorizing CCR5 residues into panels A and B. The first term in the numerator represents the interaction free energy of CCL5 residue "q" summed up for all possible interacting CCR5 residues "j". The second term in the numerator represents the interaction free energy of HIV-1 gp120 V3 loop residue "p" summed up for all possible interacting CCR5 residues "j". The denominator represents the absolute minimum value of the aforementioned terms in the numerator.

Supplementary Figures

Supplementary Figure 1

A

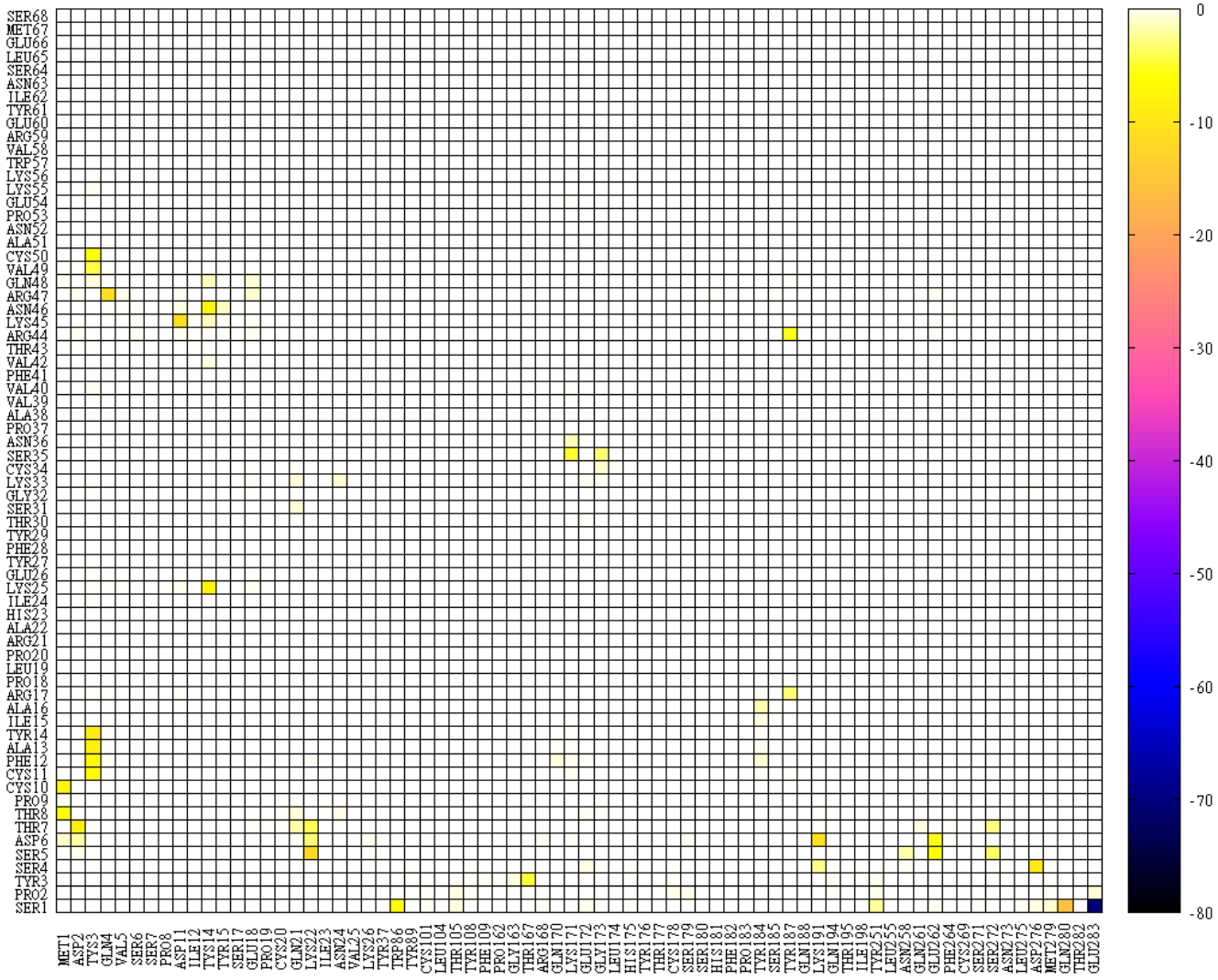

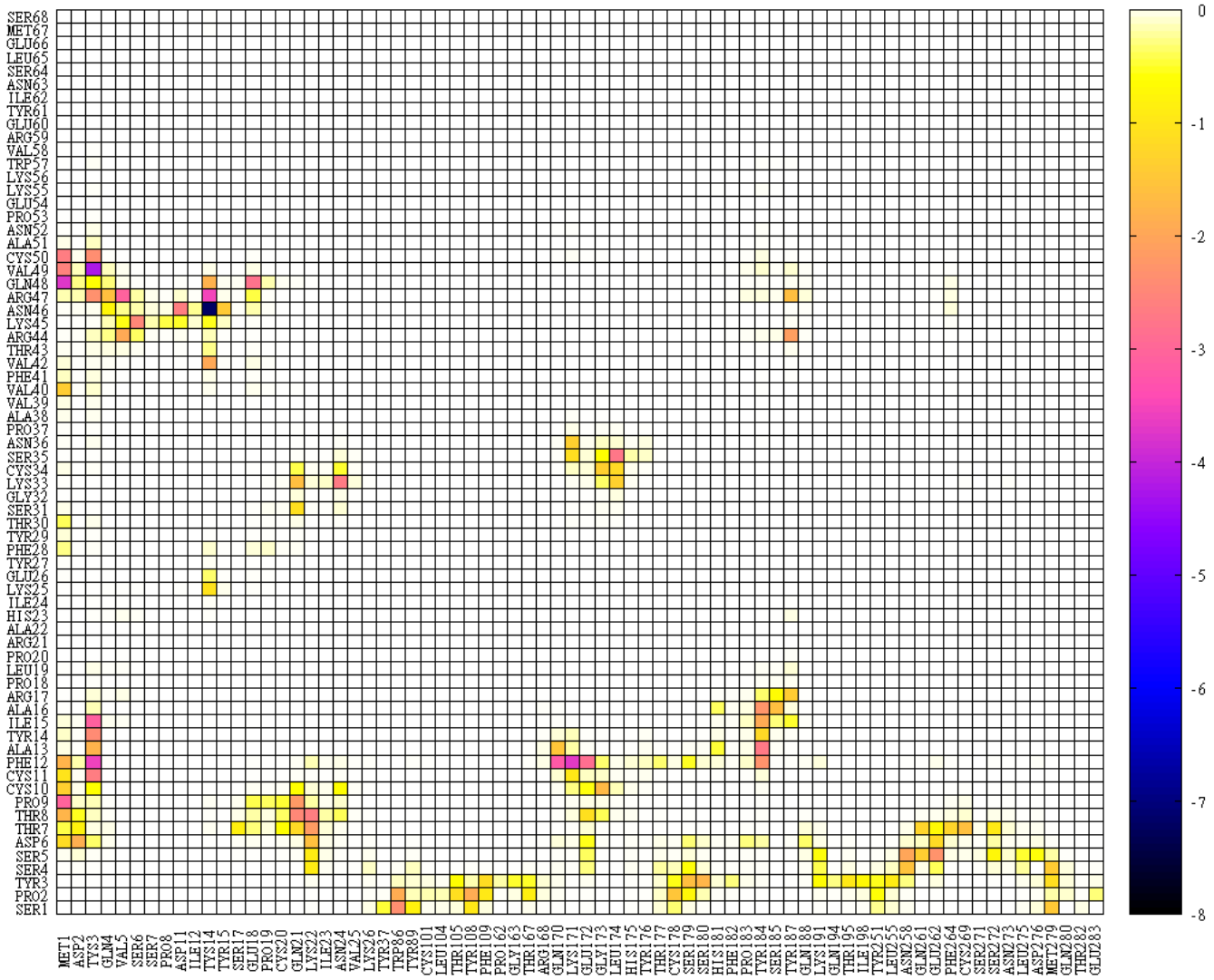

Supplementary Figure 1: Two dimensional density maps depicting the favorable (negative) average MM GBSA interaction free-energies for intermolecular CCL5 (y axis) : CCR5 (x axis) interacting residue pairs, within the simulation of the complex with the lowest average binding free energy. Panels (A) and (B) correspond to polar and non-polar interactions, respectively. All energies are in kcal/mol. The color – interaction free energy correspondence is shown by the palette on the right-hand side of each panel. All values have been computed by analysis of 1000 snapshots, extracted from the 20-ns simulation (of Complex 14A), at 20-ps intervals. Residue name "Tys" corresponds to a sulfated tyrosine.

Supplementary Figure 2

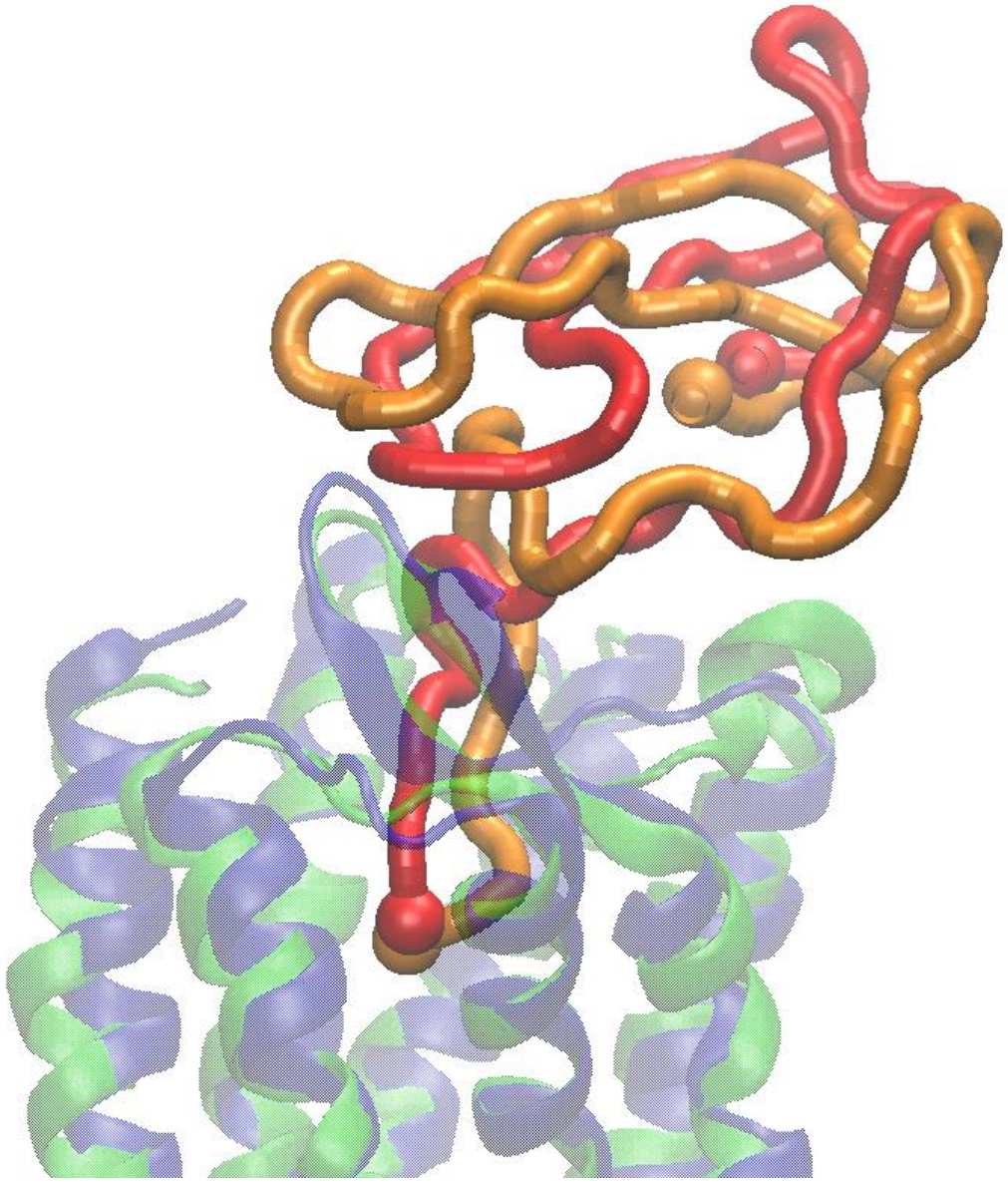

Supplementary Figure 2A: Superimposed molecular graphics images of CCL5 in complex with CCR5 and CXCL2 in complex with CXCR4[14]. The structures correspond to the final simulation snapshots of CXCL2 in complex with CXCR4[14] and CCL5 in complex with CCR5 (Complex 14A in this work). CXCL12 is shown in red color, CXCR4 is shown in blue color, CCL5 is shown in orange color, and CCR5 is shown in green color. The N-terminal domains of the chemokine receptors are not presented for clarity. Only the principal interacting chemokine residue domains 1-48 are presented. The Cα atoms of chemokine residues 1 (bottom) and 48 (top) are shown in van der Waals spheres.

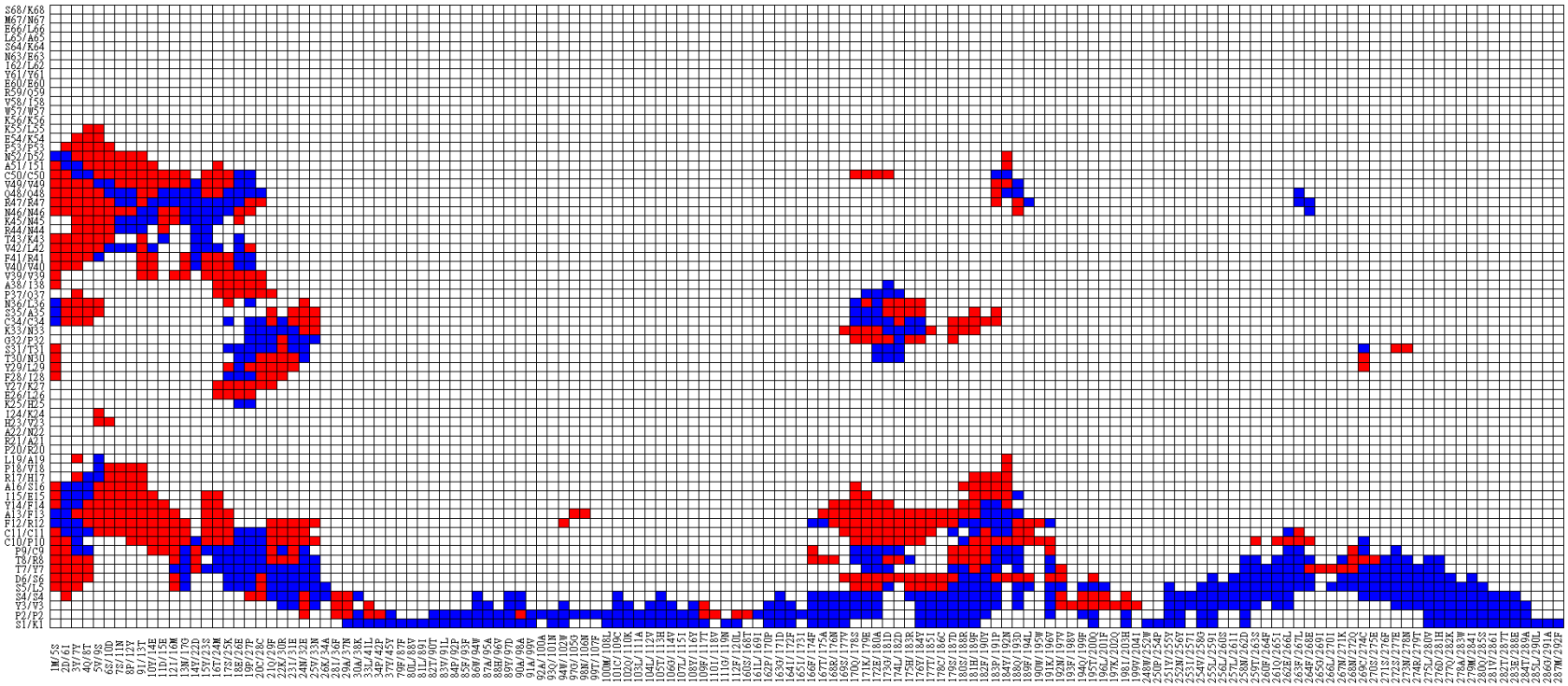

Supplementary Figure 2B: Two dimensional density map depicting the CCL5 / CXCL12 (y axis) Cα : CCR5 / CXCR4 (x axis) Cα residue pairs which are located on the protein binding interface in the final simulation snapshots of CCL5 : CCR5 and CXCL12 : CXCR4[14]. A blue color denotes that the Cα : Cα distance for the specific residue pair is similar (< 4Å) in the two complexes, whereas a red color denotes that the distance is not similar (> 4Å). Residue pairs which are denoted in white color are not part of the binding interface.

Supplementary Tables:

Supplementary Table 1

Hydrogen bond percentage (%) occupancies of important intermolecular hydrogen-bonding atom pairs within the Complex 14A simulation.

CCL5 Residue	Number	Group	Atom	CCR5 Residue	Number	Group	Atom	Occupancy (%)
SER	1	Main	N	GLN	280	Side	OE1	100
SER	1	Main	N	GLN	280	Side	NE2	9.29
SER	1	Main	N	GLN	280	Side	NE2	9.29
SER	1	Main	N	GLU	283	Side	OE1	99.9
SER	1	Main	N	GLU	283	Side	OE2	97.9
SER	1	Side	OG	TYR	251	Side	OH	95.7
SER	1	Side	OG	MET	279	Side	SD	19.58
TYR	3	Side	OH	THR	167	Side	OG1	82.92
SER	4	Main	O	LYS	191	Side	NZ	46.25
SER	4	Side	OG	LYS	22	Side	NZ	35.26
SER	4	Side	OG	ASP	276	Side	OD1	55.54
SER	4	Side	OG	ASP	276	Side	OD2	32.57
SER	5	Main	O	LYS	22	Side	NZ	96.1
SER	5	Main	N	ASN	258	Side	OD1	60.64
SER	5	Main	N	ASN	258	Side	ND2	20.78
SER	5	Side	OG	LYS	22	Side	NZ	38.46
SER	5	Side	OG	ASN	258	Side	OD1	15.88
SER	5	Side	OG	SER	272	Main	O	15.48
SER	5	Side	OG	SER	272	Side	OG	63.14
ASP	6	Main	O	MET	1	Main	N	11.39
ASP	6	Main	N	GLU	262	Side	OE2	63.94
ASP	6	Main	N	GLU	262	Side	OE1	57.44
ASP	6	Side	OD1	SER	179	Side	OG	7.79
ASP	6	Side	OD2	LYS	191	Side	NZ	77.72
ASP	6	Side	OD1	LYS	191	Side	NZ	55.24
THR	7	Main	N	ASP	2	Side	OD2	63.44
THR	7	Main	N	ASP	2	Side	OD1	11.49
THR	7	Main	O	LYS	22	Main	N	92.81
THR	7	Side	OG1	ASP	2	Side	OD2	25.17
THR	7	Side	OG1	SER	272	Side	OG	57.64
THR	8	Main	O	MET	1	Main	N	81.92
THR	8	Side	OG1	GLN	21	Side	NE2	31.17
THR	8	Side	OG1	LYS	22	Main	O	8.29
THR	8	Side	OG1	ASN	24	Side	OD1	10.49

THR	8	Side	OG1	ASN	24	Side	ND2	7.99
PRO	9	Main	O	MET	1	Main	N	13.99
CYS	10	Main	O	MET	1	Main	N	81.32
PHE	12	Main	N	TYS	3	Side	OS3	94.71
PHE	12	Main	N	TYS	3	Side	OS2	68.63
PHE	12	Main	O	GLN	170	Side	NE2	46.05
PHE	12	Main	O	LYS	171	Main	N	16.28
ALA	13	Main	N	TYS	3	Side	OS3	95.4
TYR	14	Main	N	TYS	3	Side	OS3	99.9
ALA	16	Main	N	TYR	184	Main	O	54.85
ARG	17	Side	NH1	TYR	187	Side	OH	38.06
LYS	25	Side	NZ	TYS	14	Side	OS4	23.88
LYS	25	Side	NZ	TYS	14	Side	OS3	22.68
LYS	25	Side	NZ	TYS	14	Side	OS2	20.28
SER	31	Side	OG	GLN	21	Side	OE1	32.17
SER	31	Side	OG	GLN	21	Side	NE2	13.59
LYS	33	Main	O	ASN	24	Side	ND2	17.58
LYS	33	Side	NZ	GLN	21	Side	OE1	12.29
LYS	33	Side	NZ	ASN	24	Side	OD1	7.49
SER	35	Main	N	GLY	173	Main	O	81.62
SER	35	Side	OG	LYS	171	Side	NZ	67.03
SER	35	Side	OG	GLY	173	Main	O	41.46
ASN	36	Side	OD1	LYS	171	Side	NZ	22.18
ARG	44	Side	NH1	TYR	187	Side	OH	89.71
ARG	44	Side	NH2	TYR	187	Side	OH	29.47
LYS	45	Side	NZ	ASP	11	Side	OD1	43.16
LYS	45	Side	NZ	ASP	11	Side	OD2	22.48
ASN	46	Main	N	TYS	14	Side	OS2	8.69
ASN	46	Main	N	TYS	14	Side	OS4	7.69
ASN	46	Main	N	TYS	14	Side	OS3	7.69
ASN	46	Side	ND2	ASP	11	Main	O	9.59
ASN	46	Side	ND2	TYS	14	Side	OS3	14.89
ASN	46	Side	ND2	TYS	14	Side	OS2	14.39
ASN	46	Side	ND2	TYS	14	Side	OS4	12.99
ASN	46	Side	ND2	TYR	15	Side	OH	59.54
ARG	47	Main	N	TYS	14	Side	OS2	26.47
ARG	47	Main	N	TYS	14	Side	OS4	26.27
ARG	47	Main	N	TYS	14	Side	OS3	25.37
ARG	47	Side	NE	GLN	4	Main	O	100
ARG	47	Side	NH2	GLN	4	Main	O	79.22
GLN	48	Side	NE2	TYS	14	Side	OS2	15.68

GLN	48	Side	NE2	TYS	14	Side	OS3	12.49
GLN	48	Side	NE2	TYS	14	Side	OS4	10.59
GLN	48	Side	NE2	GLU	18	Side	OE1	12.99
GLN	48	Side	NE2	GLU	18	Side	OE2	9.29
CYS	50	Main	N	TYS	3	Side	OS4	100

We sort the hydrogen bonding atom pairs, firstly, with respect to the residue number of the CCL5 atom, and secondly, the residue number of the CCR5 atom. All values have been computed by analysis of 1000 snapshots (per complex), extracted from the 20-ns of Complex 14 A, at 20-ps intervals. A hydrogen bond was present if the donor (D)–acceptor (A) distance was less than 3.5 Å and the corresponding angle (D–H ··· A) was larger than 90°. Hydrogen bond interactions associated with salt-bridge formation are consecutively highlighted in yellow background. Hydrogen bonding atom pairs with less than 8% occupancy are not reported.

Supplementary Table 2

Binding free energies using the GBSA and MM GBSA approximations for CCL5 : CCR5 complexes.

	Docking and Minimization[¶]			MD Simulations[†]		
	GBSA			MM GBSA		
	Non-Polar	Polar	Total	Non- polar	Polar	Total
1[§]	-157.0	-13.3	-170.4	-239.6 (9.5)	-69.2 (10.0)	-308.8 (10.6)
2	-145.0	-15.7	-160.7	-254.5 (12.3)	-57.7 (12.2)	-312.2 (16.1)
3	-130.0	-28.0	-158.0	-218.2 (12.3)	-69.0 (11.5)	-287.2 (11.5)
4	-152.3	-5.6	-157.9	-262.2 (18.2)	-63.1 (12.9)	-325.3 (18.2)
5	-146.1	-11.0	-157.1	-227.6 (9.1)	-88.9 (11.5)	-316.5 (12.9)
6	-136.4	-18.0	-154.4	-223.6 (8.8)	-79.5 (13.6)	-303.1 (14.0)
7	-129.9	-23.6	-153.5	-218.7 (10.4)	-53.9 (8.9)	-272.6 (10.9)
8	-132.0	-20.0	-152.1	-233.9 (8.8)	-75.9 (11.9)	-309.7 (12.8)
9	-138.7	-13.0	-151.8	-215.0 (8.2)	-75.9 (13.3)	-290.9 (14.0)
10	-130.2	-19.8	-150.0	-213.0 (11.0)	-71.7 (11.3)	-284.7 (12.6)
11	-153.7	4.0	-149.7	-205.4 (9.8)	-79.9 (12.5)	-285.1 (11.9)
12	-138.5	-11.1	-149.6	-245.0 (8.9)	-85.6 (12.9)	-330.7 (13.4)
13	-115.0	-33.2	-148.3	-237.6 (7.3)	-79.3 (9.8)	-316.8 (9.5)
14	-129.4	-18.6	-148.0	-242.2 (11.4)	-103.9 (12.3)	-346.1 (16.0)
15	-141.8	-6.2	-148.0	-233.3 (8.4)	-30.0 (9.5)	-263.3 (10.6)
16	-124.5	-23.2	-147.6	-218.0 (9.2)	-58.4 (10.7)	-276.4 (13.2)
17	-125.0	-22.6	-147.6	-249.7 (8.4)	-90.4 (11.7)	-340.1 (11.2)
18	-135.4	-11.9	-147.4	-220.9 (9.4)	-74.6 (12.7)	-295.4 (13.3)
19	-130.5	-16.7	-147.2	-253.4 (8.7)	-67.8 (11.4)	-321.2 (11.1)
20	-123.3	-23.8	-147.1	-230.8 (9.8)	-71.2 (12.1)	-302.0 (11.5)
21	-123.7	-23.4	-147.1	-224.0 (9.3)	-80.0 (11.9)	-304.0 (11.4)
22	-122.4	-24.4	-146.7	-193.8 (8.1)	-72.7 (10.8)	-266.5 (9.7)
23	-125.6	-21.0	-146.6	-223.0 (8.1)	-46.8 (11.9)	-269.8 (12.4)
24	-152.2	5.6	-146.6	-259.4 (8.0)	-49.9 (10.8)	-309.3 (9.5)
25	-146.9	0.5	-146.5	-220.4 (7.4)	-71.5 (9.8)	-291.9 (10.0)
14A	---	---	---	-244.2 (8.3)	-105.9 (10.5)	-**350.1** (11.0)
17A	---	---	---	-253.5 (8.5)	-83.7 (11.2)	-337.1 (12.2)

The binding free energies (kcal/mol) are calculated as described in Methods. The numbering[§] (1-25) is sorted according to the total binding free energy, using the GBSA approximation, of the docked complexes after minimization, referred as step 4[¶]; the total binding free energy is the sum of non-polar and polar contributions of step 4. The MD simulation[†] results correspond to the

average binding free energies of the 25 complexes, based on 30-ns MD simulation runs, as well as the additional simulations “14A” and “17A”, based on 20-ns MD simulation runs, referred as steps 5 and 6, respectively. The values were calculated using the MM GBSA approximation, decomposed into non-polar and polar contributions of step 6. The standard deviation is shown in parentheses. Complexes 14 and 17 are highlighted in gray background as they possess the lowest binding free energy from all 25 Complexes. Complex 14A is also highlighted as it possesses the lowest binding free energy among all complexes; also, the total binding free energy of simulation “14A” is shown in **bold** face. All MD simulation values have been computed by analysis of 1000 snapshots, extracted from the last 20-ns simulations (of all complexes), at 20-ps intervals.

Supplementary Coordinates

The MD coordinates of the final simulation, extracted every 2-ns are provided as Supplementary Coordinates in PDB format. The structures are aligned with regard to the backbone of the CCR5 transmembrane helical region. The correspondence of PDB files and time in the MD simulation is as follows:

PDB file	Time (ns)
ccl5_ccr5.1.pdb	2
ccl5_ccr5.2.pdb	4
ccl5_ccr5.3.pdb	6
ccl5_ccr5.4.pdb	8
ccl5_ccr5.5.pdb	10
ccl5_ccr5.6.pdb	12
ccl5_ccr5.7.pdb	14
ccl5_ccr5.8.pdb	16
ccl5_ccr5.9.pdb	18
ccl5_ccr5.10.pdb	20

Supplementary Video

A video demonstrating the final simulation trajectory of CCL5 : CCR5, and depicting the gradual stabilization and preservation of the key salt bridges, important hydrogen bonds and important cation-π interactions, which are shown in Figure 2, is provided as Supplementary Information.

Supplementary References

[1] Schnur, E. et al. NMR mapping of RANTES surfaces interacting with CCR5 using linked extracellular domains. *FEBS J.* 280, 2068-2084 (2013).

[2] Schnur, E. et al. The conformation and orientation of a 27-residue CCR5 peptide in a ternary complex with HIV-1 gp120 and a CD4-mimic peptide. *J Mol Biol.* 410, 778-797 (2011).

[3] Tamamis, P. & Floudas, C. A. Molecular recognition of CCR5 by an HIV-1 gp120 V3 loop. *PLoS ONE* 9(4): e95767 (2014).

[4] Chung, C. W., Cooke, R. M., Proudfoot, A. E. & Wells, T. N. The three-dimensional solution structure of RANTES. *Biochemistry*. 34, 9307-9314 (1995).

[5] Wang, X., Watson, C., Sharp, J. S., Handel, T. M. & Prestegard, J. H. Oligomeric structure of the chemokine CCL5/RANTES from NMR, MS, and SAXS data. *Structure.* 19, 1138-1148 (2011).

[6] Choi, W. T. et al. CCR5 mutations distinguish N-terminal modifications of RANTES (CCL5) with agonist versus antagonist activity. *J. Virol.* 86, 10218-10220 (2012).

[7] Proudfoot, A. E. et al. Extension of recombinant human RANTES by the retention of the initiating methionine produces a potent antagonist. *J. Biol. Chem.* 271, 2599-2603 (1996).

[8] Govaerts, C. et al. Activation of CCR5 by chemokines involves an aromatic cluster between transmembrane helices 2 and 3. *J Biol Chem.* 278, 1892-1903 (2003).

[9] Kondru, R. et al. Molecular interactions of CCR5 with major classes of small-molecule anti-HIV CCR5 antagonists. *Mol Pharmacol.* 73, 789-800 (2008).

[10] Blanpain, C. et al. The core domain of chemokines binds CCR5 extracellular domains while their amino terminus interacts with the transmembrane helix bundle. *J. Biol. Chem.* 278, 5179-5187 (2003).

[11] Maeda, K., Das, D., Ogata-Aoki, H., Nakata, H., Miyakawa, T., Tojo, Y., Norman, R., Takaoka, Y., Ding, J., Arnold, G. F., Arnold, E. & Mitsuya, H. Structural and molecular interactions of CCR5 inhibitors with CCR5. *J. Biol. Chem*. 281, 12688-12698 (2006).

[12] Tan, Q., Zhu, Y., Li, J., Chen, Z., Han, G. W., Kufareva, I., Li, T., Ma, L., Fenalti, G., Li, J., Zhang, W., Xie, X., Yang, H., Jiang, H., Cherezov, V., Liu, H., Stevens, R. C., Zhao, Q. & Wu, B. Structure of the CCR5 chemokine receptor-HIV entry inhibitor maraviroc complex. *Science.* 341, 1387-1390 (2013).

[13] Tamamis, P. & Floudas, C. A. Molecular recognition of CXCR4 by a dual tropic HIV-1 gp120 V3 loop. *Biophys J.* 105, 1502-1514 (2013).

[14] Tamamis, P. & Floudas, C. A. Elucidating a Key Component of Cancer Metastasis: CXCL12 (SDF-1α) Binding to CXCR4. *J. Chem. Inf. Model*. 54 (4), 1174-1188 (2014).

[15] Tamamis, P., Morikis, D., Floudas, C. A. & Archontis, G. Species specificity of the complement inhibitor compstatin investigated by all-atom molecular dynamics simulations. *Proteins*. 78, 2655-2667 (2010).

[16] Tamamis, P. et al. Design of a modified mouse protein with ligand binding properties of its human analog by molecular dynamics simulations: the case of C3 inhibition by compstatin. *Proteins*. 79, 3166-3179 (2011).

[17] Tamamis, P. et al. Molecular dynamics in drug design: new generations of compstatin analogs. Chem. Biol. Drug. Des. 79, 703-718 (2012).

[18] Gorham, R. D. et al. Novel compstatin family peptides inhibit complement activation by drusen-like deposits in human retinal pigmented epithelial cell cultures. *Exp. Eye. Res.* 116, 96-108 (2013).

[19] Kieslich, C. A. et al. Exploring protein-protein and protein-ligand interactions in the immune system using molecular dynamics and continuum electrostatics. *Current Physical Chemistry*. 2, 324-343 (2012).

[20] Im, W., Feig, M. & Brooks, C. L. III. An implicit membrane generalized born theory for the study of structure, stability and interactions of membrane proteins. *Biophys. J.* 85, 2900-2918 (2003).